A solar powered handheld plasma source for microbial decontamination applications

You may also be interested in:

Ozone correlates with antibacterial effects from indirect air dielectric barrier discharge treatment of water
Matthew J Pavlovich, Hung-Wen Chang, Yukinori Sakiyama et al.

Quantification of air plasma chemistry for surface disinfection
Matthew J Pavlovich, Douglas S Clark and David B Graves

Air spark-like plasma source for antimicrobial NOx generation
M J Pavlovich, T Ono, C Galleher et al.

A battery-operated atmospheric-pressure plasma wand for biomedical applications
X Pei, J Liu, Y Xian et al.

Momentum, heat, and neutral mass transport in convective atmospheric pressure plasma-liquid systems and implications for aqueous targets
Alexander Lindsay, Carly Anderson, Elmar Slikboer et al.

Atmospheric pressure dielectric barrier discharges interacting with liquid covered tissue
Wei Tian and Mark J Kushner

A solar powered handheld plasma source for microbial decontamination applications

Y Ni[1,4]**, M J Lynch**[1,4]**, M Modic**[1,2]**, R D Whalley**[3] **and J L Walsh**[1]

[1] Department of Electrical Engineering and Electronics, University of Liverpool,
Brownlow Hill, Liverpool L69 3GJ, UK
[2] Department of Surface Engineering and Optoelectronics, Institute 'Jožef Stefan',
Jamova 39, 1000 Ljubljana, Slovenia
[3] School of Mechanical and Systems Engineering, Newcastle University, NE1 7RU, UK

E-mail: jlwalsh@liverpool.ac.uk

Abstract

A fully portable atmospheric pressure air plasma system is reported to be suitable for the microbial decontamination of both surfaces and liquids. The device operates in quiescent air, and includes an integrated battery which is charged from a solar cell and weighs less than 750 g, making it highly amenable for a wide variety of applications beyond the laboratory. Using particle imaging velocimetry to visualise air flows around the device, the geometric configuration of the plasma generating electrodes was enhanced to induce a gas flow on the order of 0.5 m s^{-1} directed towards a sample placed downstream, thus improving the transport of plasma generated reactive species to the sample. The microbial decontamination efficiency of the system was assessed using potable water samples inoculated with common waterborne organisms *Escherichia coli* and *Pseudomonas fluorescens*. The reduction in the number of microorganisms was found to be in the range of 2–8 log and was strongly dependent on the plasma generation conditions.

Keywords: surface barrier discharge, atmospheric pressure, non-thermal air plasma

(Some figures may appear in colour only in the online journal)

1. Introduction

The generation of non-equilibrium plasma at atmospheric pressure produces a rich variety of reactive chemical species at low temperatures which are unbound by the confines of a vacuum chamber. Plasmas generated in the ambient air have shown great promise for low-cost, consumable-free, decontamination applications where plasma generated reactive oxygen and nitrogen species (RONs) interact with contaminants resulting in rapid oxidation/inactivation on both solid surfaces and in aqueous volumes [1–4]. In particular, the use of plasma for water decontamination has proven extremely effective with a large number of studies demonstrating the

ability of plasma to inactivate microorganisms and break down persistent chemicals directly in liquid [5–7]. Water supplies containing chemical contaminants and/or pathogenic bacteria pose a risk to over 780 million people globally; contributing to ∽10% of the total burden of disease worldwide. According to the World Health Organization this dire situation could be prevented through improvements related to drinking-water, sanitation, hygiene and water resource management [8]. The scale of the challenge is enormous; with ∽88% of cases of diarrhea worldwide attributed to unsafe water, inadequate sanitation or insufficient hygiene. These cases result in 1.5 million deaths each year, most being the deaths of children and many of which occur in low-income and developing countries [9]. While conventional water purification technologies, including chlorine treatment and membrane filtration, are highly effective and help save millions of lives each year, they do not offer a consumable free option and may be difficult to obtain in remote locations or in emergency situations. As such, there is

[4] Authors contributed equally.

J. Phys. D: Appl. Phys. **49** (2016) 355203

Y Ni *et al*

a real need to develop low-cost water treatment technologies that can be used indefinitely in remote locations and emergency situations without the need for consumables. Given the 'consumable-free' nature of atmospheric pressure air plasma decontamination, such systems could play a significant role in addressing this need, especially as they are low-cost to construct and can be scaled with ease [10].

In the context of plasma mediated liquid decontamination, two common approaches include plasma generation directly in the liquid (usually within bubbles) and plasma generation above the liquid surface [6, 7]. While the generation of plasma directly in liquid offers the highest possible transfer of plasma species to the liquid phase, the plasma properties are strongly dependent on the electrical properties of the liquid, greatly adding to the complexity of the system. Plasmas generated above the liquid can directly interact with the liquid surface or be remote, relying on diffusion to transport species from the plasma region to the liquid [4, 6]. In the remote case, plasma generation is immune to changes in the electrical properties of the liquid which is a distinct advantage; however, the separating gas layer essentially inhibits the transfer of the most reactive plasma generated species which ultimately reduces the application efficiency, a distinct disadvantage [6]. Several studies have explored the development of portable plasma systems that are suitable for microbial decontamination and materials processing applications. Typically these devices take the form of a plasma-jet, where a flowing gas is ionised and flushed towards a sample placed downstream of the plasma generating electrodes; noble gases such as helium or argon can be used and are typically supplied by an external compressed gas cylinder [11]. Alternatively, ambient air can be used by making use of a miniature pumping system [12]. Recently, Pai *et al* reported a battery operated 'plasma-wand' system employing a dielectric barrier electrode protruding from the device and operating in quiescent air, thus doing away with the need to pump gas through the device [13].

This contribution details the development of a portable plasma device based on a large area Surface Barrier Discharge (SBD), which is chosen due to its ease of implementation and its ability to generate high concentrations of RON species [14]. Typically, portable plasma systems rely on an integrated battery that, once fully discharged, is replaced or connected to an external power source to be replenished. The device reported here does away with the need for any external power source by making use of an integrated solar charging unit, thus enabling operation in remote locations or emergency situations where no external power source is available. When the device is activated a discharge forms on the dielectric surface of the electrode, the device is typically placed several millimeters above the sample requiring decontamination. A consequence of this spatial separation between the plasma generation region and the application region is a reduced mass-transfer of reactive plasma species to the sample [6]. To improve mass-transport, particle imaging velocimetry (PIV) was used to visualise the flow patterns around the electrode, enabling the electrode geometry to be optimised to yield a gas flow perpendicular to the electrode unit, thus enhancing the transport of reactive species from the electrode to the sample. For
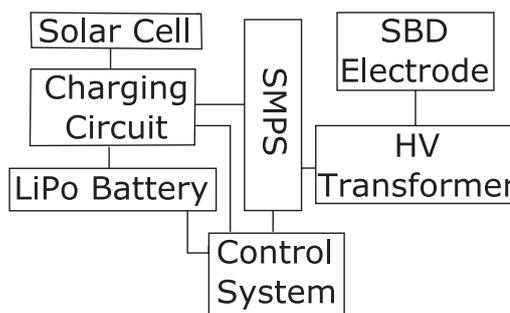

Figure 1. Electrical sub-systems within the portable plasma source.

the decontamination experiments considered in this investigation, potable water samples inoculated with the common waterborne organisms *Escherichia coli* and *Pseudomonas fluorescens* were treated using the plasma system for various periods of time. It was found that the level of decontamination was strongly dependent on the plasma generation conditions and that pulse modulation of the plasma offered a viable means to decontaminate liquid samples without inducing undesirable changes in the liquid pH.

The remainder of the manuscript is organised as follows: section 2 details the plasma source design, section 3 provides the experimental setup, section 4 presents the results obtained and accompanying discussion, and finally section 5 provides concluding remarks.

2. Plasma source design

The plasma source used in this study was developed in-house and comprised of a flexible solar cell, a 2 cell lithium-polymer (LiPo) battery, a microprocessor control system and high-voltage generation circuitry. Figure 1 shows a block diagram of the device.

During operation, the microprocessor control system monitors the charging of the LiPo battery from the solar panel and is able to switch between a charge and discharge mode of operation at the press of a button situated on the handle of the device. When the discharge mode of operation is selected, battery charging ceases and the output of the LiPo battery is directed to the switched mode power source (SMPS) unit. In the SMPS unit a boost converter is used to step-up the nominal 7.4 V provided by the LiPo battery to 30 V; a MOSFET half-bridge subsequently chops the 30 V DC signal into a high frequency square wave which is suitable for driving a miniature high-voltage transformer. The output of the transformer is connected directly to the SBD electrodes. The driving frequency automatically adjusts to the natural resonant frequency of the transformer secondary and electrode capacitance, including the stray capacitances/inductances within the system. The microprocessor control system also facilitates a pulse modulated mode of operation, whereby plasma was generated for 25 ms in every 100 ms period thus giving a duty-cycle of 25%. The SBD electrode comprised of a 100 mm diameter, 1 mm thick quartz disc, with patterned aluminium electrodes adhered either side; the specific design of the electrodes is discussed later. To house the plasma generation electronics

J. Phys. D: Appl. Phys. **49** (2016) 355203

Y Ni *et al*

Figure 2. Portable air plasma device operating in a continuous mode of operation at 10 W dissipated power.

Figure 3. (a) Voltage and current characteristics of the charging process of the LiPo battery using the integrated solar panel. (b) Applied voltage and measured current under continuous operation.

and electrode unit an enclosure was fabricated from polylactic acid (PLA) using a 3D printer, the enclosure was designed to incorporate the flexible solar panel in the handle of the device. The complete plasma system, including electrode unit, electronics and solar cell weighs less than 750 g and comfortably fits in the palm of the hand, shown in figure 2.

When charging the battery from the solar cell, it was established that a typical charge time from a discharged state was approximately 10 h when the system was placed within a well-lit room, as shown in figure 3(a). With the battery fully charged, it was found that a plasma dissipating 10 W could be sustained continuously for approximately 1 h; suggesting an efficiency on the order of 85% which is not uncommon for switched mode power sources of this nature. In a pulse modulated mode of operation, with a duty-cycle of 25%, it is estimated that a ∼3 h window of operation would be possible. Figure 3(b) shows the applied voltage and current during continuous operation at 40 kHz. Such waveforms are highly typical of an SBD excited from a kHz frequency sinusoidal source. While the applied voltage remains sinusoidal, the measured current shows numerous 'spikes', each representing a single plasma filament. These spikes are superimposed upon a displacement current that is 90 degrees out of phase with the applied voltage, highlighting the capacitive nature of the electrode unit.

3. Experimental setup

3.1. Particle image velocimetry

Global measurements of the velocity field were taken along the centreline of the SBD electrode with a time-resolved particle image velocimetry (PIV) system from TSI Incorporated. All measurements were conducted inside a closed chamber to ensure the plasma generated air flow was not influenced
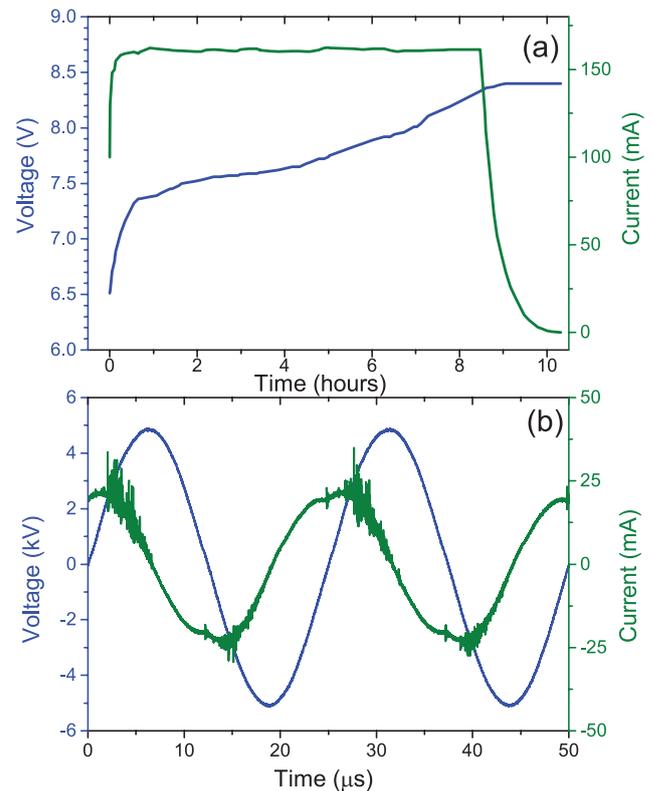
by any external drafts. The chamber had a cross-section of 1000 mm × 1000 mm and a height of 1500 mm. The PIV system consisted of a Photron Fastcam APX camera (1024 × 1024 pixels), a New Wave Research Pegasus PIV laser and a TSI 9307-6 oil droplet generator. Olive oil with a nominal size of 1 μm was used to seed the air within the closed chamber. The camera was set to view an area of 80 mm × 80 mm, and 500 image pairs were acquired at a frequency of 500 Hz, with a time delay between frames being typically 200 μs. Data processing was performed with INSIGHT 3G software from TSI using a recursive cross-correlation algorithm to generate vectors on a 32 × 32 pixel interrogation area with a 50% overlap, providing velocity data with a 1 mm spatial resolution to an accuracy of 3–5% [15]. The Stokes numbers of the seeding particles used throughout this study was <0.1. This ensured that the seeding particles followed the fluid flow closely with tracing errors being <1% [16].

3.2. Microbial decontamination

Bactericidal properties of the plasma system were evaluated using two different bacterial species, both commonly found in water systems, *E. coli* (NCIMB 12413) and *Pseudomonas fluorescens* (NCIMB 9046). Bacterial solutions were prepared with autoclaved tap water to obtain an initial concentration of approximately 10^8 colony-forming units per ml (CFU · ml^{-1}). A 25 ml sample of each suspension was transferred to a petri dish prior to plasma exposure. During plasma exposure, the plasma source was placed on top of the petri dish containing

the liquid sample for the duration of the treatment. The discharge power was monitored continuously throughout the treatment by measuring the applied voltage and current to calculate the instantaneous power, which was averaged over many applied voltage cycles using a 1 GHz bandwidth large memory oscilloscope [6]. Different exposure times were used according to the plasma regime under investigation; in a continuous plasma generation mode of operation (10 W dissipated power), plasma exposure times included 30 s, 1 min, 2 min, 3 min and 4 min. In a pulse modulated mode of operation, with a duty cycle of 25% (2.5 W dissipated power), exposure times of 2, 4, 8, 12 and 16 min were considered. Treatment times in the pulsed modulated case were chosen such that they are directly comparable in terms of energy use to the continuous treatments. In all cases, gentle stirring was used to enhance species transport in to the bulk liquid phase. The temperature of the liquid was measured at the end of each test and was found not to exceed 25 °C under any of the plasma generation conditions considered. All treatments were conducted in triplicate. Immediately after treatment suspensions were serially diluted and plated on Tryptic Soy Agar. The Agar plates were incubated overnight at 37 °C (*E. coli*) and 26 °C (*P. fluorescens*). The number of counted colonies on each Agar plate was used to determine the level of bacterial survival, information which was converted to a log reduction using the standard approach [17].

3.3. Gas phase species quantification

Long-lived gas phase species were measured using Fourier transform infra red (FTIR) spectroscopy. The electrodes were placed within a sealed enclosure with a volume similar to that used in the microbiology experiments and plasma was generated using the same conditions as those used in the microbiology tests (detailed in section 3.2). After each test, the effluent within the sealed enclosure was drawn into an FTIR gas cell (multi-pass design with 16 m path length) using a small vacuum pump. A Jasco FT/IR-4000 spectrometer with a mid-IR optical bench from 7800 cm^{-1} to 500 cm^{-1} was used to record the resulting IR absorption spectrum. For each measurement, the resolution for data acquisition was set to 4 cm^{-1} and each spectra comprised of 25 individual acquisitions averaged. Following each measurement, the system was exhausted in to a fume extraction unit and the measurement system flushed for several minutes with laboratory air to remove plasma species from the gas cell and electrode enclosure.

The concentration of gaseous phase species were estimated by fitting the FTIR absorption peaks for each molecule with standard reference profiles obtained from the Pacific Northwest National Laboratory (PNNL) [18]. The standard reference data was collected at 1 part-per-million-meter (ppm-meter) resolution at 296 K with a path length of 1 m. To obtain the concentration (C) of a particular molecule from the absorption spectra, the equation $C = A/(B.l)$ was used, where A is the area of the FTIR peak of a particular specie, B is the standard peak area and l is the difference between the experimental gas cell path length and the path length used to obtain the reference data. To supplement the FTIR

measurements time-resolved ozone density was measured using an ozone monitor from 2B technologies, model 106-M.

4. Results and discussion

4.1. Species transport and optimization

A potential drawback of the SBD configuration is the limited mass-transfer of reactive plasma species from the plasma region to the sample. Sakiyama *et al* conducted a computational study to investigate the transport of plasma species in the afterglow region of an air SBD and it was hypothesized that the introduction of a convective flow on the order of 10 m s^{-1} could greatly improve the mass-transport of species beyond the discharge region, enabling species such as N, O, OH and NO to reach a sample surface situated 1 mm from the discharge [19]. It is well known that dielectric barrier discharges, excited using either sinusoidal or pulsed excitation, are capable of generating air flow velocities of several m s^{-1}; this phenomena is attributed to the electro-hydrodynamic (EHD) effect of the plasma and has been widely exploited for aerodynamic flow control applications [20]. Typically, the electrode geometry used in such studies comprises of a single strip electrode attached to a dielectric surface with a counter electrode attached to the opposite side of the dielectric material (thus forming an SBD). Operating this arrangement in quiescent air typically results in a filamentary plasma, Boeuf *et al* provided an approximate expression to calculate the EHD force generated under such conditions as $f \approx \varepsilon_0 V^2 s^{-3}$, where V is the potential drop in the cathode sheath and s is the sheath length, although difficult to measure such parameters, numerical studies have shown that the range of forces expected to be on the order of $5 \times 10^2 \sim 5 \times 10^4$ N · m^{-3} [21], with resulting velocities in the m s^{-1} range. In such an arrangement, initiation of the discharge in quiescent air creates a starting vortex which moves along and away from the electrode in a direction parallel to the dielectric surface [22]. However, for the application reported here, it is desirable for the reactive plasma species to be transported perpendicular to the dielectric surface and towards the sample. In order to achieve this, two electrodes are placed side-by-side on the dielectric surface (see schematic in figure 4), such that a discharge forms in the gap between the two electrodes. On initiation of the discharge two starting vortices are created, which move toward one another, collide, and lift vertically away from the dielectric surface by vortex induction [23]. Under continual plasma forcing, the two counter-rotating vortices are followed by a jet flow, which also moves vertically away from the dielectric surface: see figure 4, which shows the ensemble-averaged velocity field around one set of electrodes. Here, data close to the wall is omitted due to the glare caused by the laser reflection on the dielectric surface. In order to scale the device, multiple electrodes are placed side-by-side, thus creating multiple jets directed perpendicularly from the dielectric surface and towards the sample. It should be noted that the jets are always created perpendicular to the dielectric surface irrespective of the device orientation.
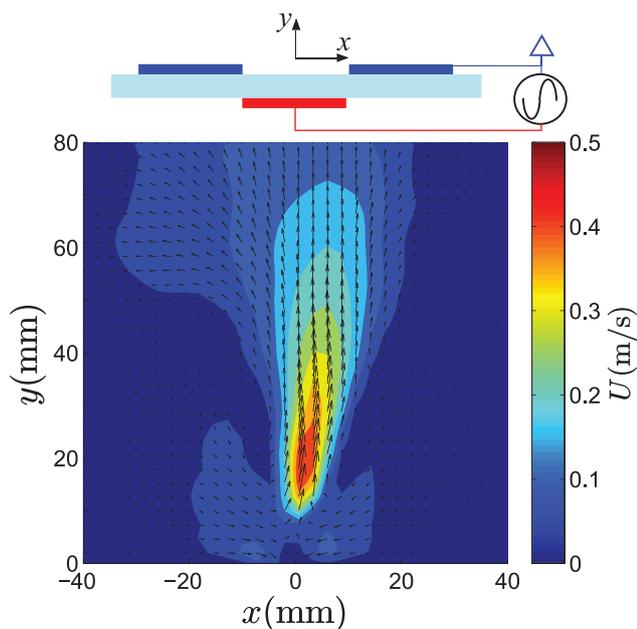
Figure 4. Ensemble-averaged velocity magnitude generated by the air plasma device operating at an applied voltage 9.7 kV$_{pp}$ with a 10 mm electrode spacing. Schematic shows the double-strip DBD actuator with the lower powered electrode highlighted in red and the upper grounded electrodes highlighted in blue.

When using parallel strip electrodes the spacing between the two facing electrode edges is a key factor in determining the velocity of the flow downstream of the dielectric surface. If the gap between the two opposing electrodes is small (e.g. 5 mm, as shown in figure 5), the length of each discharge is limited which results in a lower induced velocity. In addition, as the wall jets travel over the dielectric surface the jet half-width increases, and energy is dissipated through skin-friction drag, which results in a lower induced velocity downstream of the discharge. Figure 5 shows the impact of the spacing between two strip electrodes at various applied voltages. Taking the 10.7 kV$_{pp}$ case as an example, it is clear that the peak velocity is achieved at an electrode spacing of 15 mm; away from the optimum spacing the downstream velocity of the flow rapidly falls away. This trend is similar at 9.7 kV$_{pp}$, whereas at 8.5 kV$_{pp}$ plasma is only partially generated along the length of the electrode, compromising the flow generation efficiency. Enhancing the electrode geometry to improve the mass transport of plasma generated species to a downstream location is clearly advantageous for any application which relies on their subsequent reaction at the gas-surface interface. On the other hand, separating the electrodes by a significant distance ultimately means fewer strips can be placed within a given area, resulting in a lower density of plasma species produced. Clearly it is necessary to strike a compromise between the spacing of electrodes and the amount of plasma coverage in a given area. For the plasma device considered here, an electrode spacing of 1 cm was chosen to give a compromise between efficient mass transfer (with flow velocities in the 0.3–0.6 m s^{-1} range) whilst still generating a significant amount of plasma (1950 mm^2 of plasma coverage on the 100 mm diameter dielectric disc at a 10 W operating power).
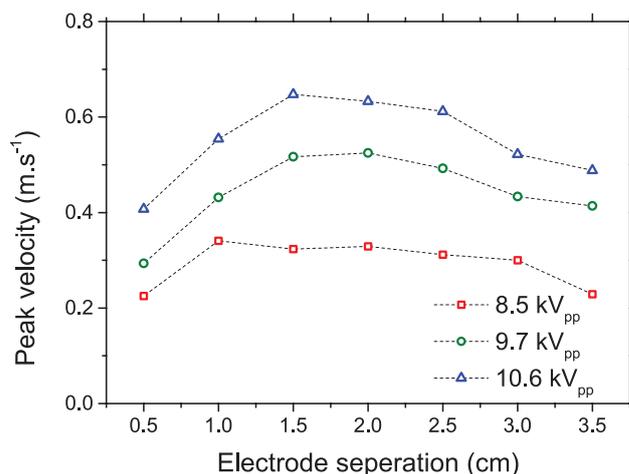

Figure 5. Peak velocity measured downstream of a single electrode pair as a function of electrode separation, at applied voltages of (triangles) 10.6 kV$_{pp}$, (circles) 9.7 kV$_{pp}$ (squares) 8.5 kV$_{pp}$.

By choosing an electrode separation of 10 mm, rather than the optimum 15 mm observed in figure 5, enabled six electrode pairs of varying length to be attached to the circular dielectric surface. A key benefit of the electrode geometry considered here is that the jet flows observed from the electrode unit are well defined and directed towards the sample region, with velocities typically five times higher in magnitude than those observed from the widely used hexagonal mesh electrodes typically found in many SBD system (data not shown).

4.2. Gas phase chemistry analysis

Numerous experimental and theoretical studies have examined the composition of plasma generated RON species in the downstream region of a SBD. A numerical study conducted by Liu *et al* considering 53 air plasma species involved in 624 reactions indicated that very few plasma generated species propagate beyond the discharge region. Following 100 s of plasma generation only hydrogen peroxide, ozone and the oxides of nitrogen (NO$_2$, NO$_3$ and N$_2$O$_5$) were found to be present 1 mm downstream of the plasma generation region at a concentration above 10^{17} m^{-3} (noting that the model only accounted for the diffusive transport of neutral species) [14]. In the experiments reported here the spatial separation between the liquid surface and the SBD electrode was fixed at ∼2 mm, with the enhanced convective flow provided by the optimised electrode geometry (∼ 0.5 m · s^{-1}) it is possible that plasma species such as nitric oxide and hydroperoxyl radicals do reach the liquid surface, introducing additional microbial inactivation pathways thus increasing the antimicrobial effects of the plasma treatment. It is well known that the chemical composition in the separating gas layer is extremely sensitive to the plasma generation conditions. Under low input power conditions (<0.2 W · cm^{-2}) the gas phase chemistry is known to be dominated by reactive oxygen species, typically ozone [4]. Under high input power conditions (>0.25 W · cm^{-2}) the gas phase chemistry is typically dominated by reactive nitrogen species, in the form of nitrogen dioxide and nitrous oxide [4]. This significant shift in chemical composition of the gas phase has been attributed to several possible
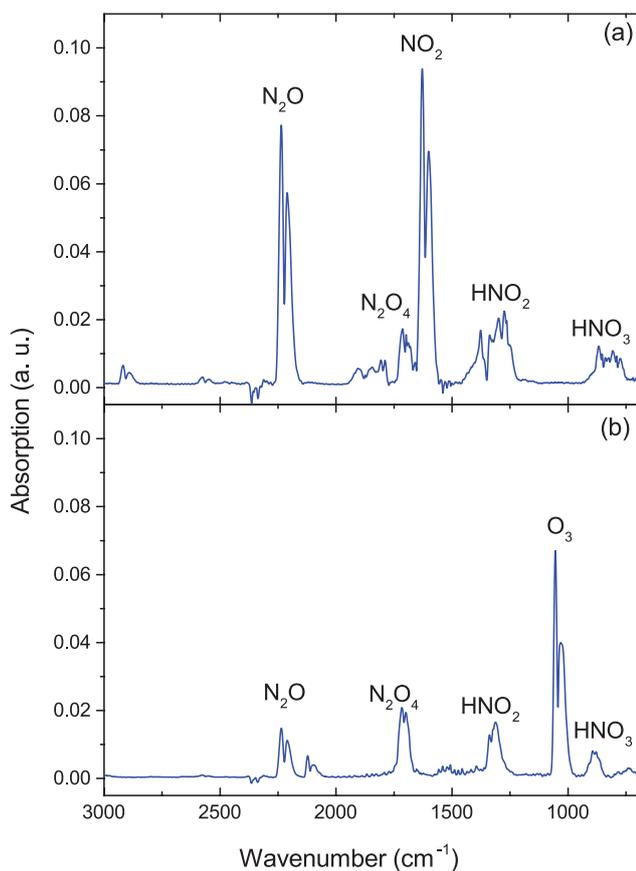
Figure 6. FTIR absorption spectra of the gas phase composition obtained using: (a) continuous operation ($0.51 \, \text{W} \cdot \text{cm}^{-2}$) and (b) pulse modulated operation ($0.13 \, \text{W} \cdot \text{cm}^{-2}$).

Figure 7. Temporal variation of nitrous oxide and ozone during pulsed modulated ($0.127 \, \text{W} \cdot \text{cm}^{-2}$) and continuous ($0.51 \, \text{W} \cdot \text{cm}^{-2}$) operation.

mechanisms, including the increased thermal decomposition of ozone at elevated temperatures and the poisoning of ozone due to elevated nitric oxide production in the discharge at higher operating powers. Shimizu *et al* proposed that vibrationally excited nitrogen, produced under high-power operating conditions, leads to an increased rate of nitric oxide formation through the reaction $N_2(v) + O \rightarrow NO + N$ ($k = 1 \times 10^{-17} \, \text{m}^3 \cdot \text{s}^{-1}$), which consumes atomic oxygen and quenches ozone formation through the reaction $O_3 + NO \rightarrow NO_2 + O_2$ ($k = 1.9 \times 10^{-20} \, \text{m}^3 \cdot \text{s}^{-1}$) [24]. Indeed, Eliasson *et al* indicate that nitric oxide and nitrogen dioxide can act catalytically in the presence of ozone and atomic oxygen to quench ozone-producing reactions, such that a very small concentration of nitric oxide and/or nitrogen dioxide can consume the ozone present in the system and inhibit further ozone production [25, 26].

In the plasma system considered here, the power dissipated within the plasma was fixed at 10 W by varying the applied voltage, this gave a power per unit area of surface coverage of $0.51 \, \text{W} \cdot \text{cm}^{-2}$, putting the device directly within the nitrogen dominated mode of operation. FTIR analysis of the gas phase species confirms this, as shown in figure 6(a). Critically, previous experimental and theoretical studies have demonstrated that the production of abundant RON species in the gas phase above a liquid layer ultimately results in the production of nitrates and nitrites in the liquid with an associated and significant drop in pH [6, 14]. In the context of the intended application, i.e. the microbial decontamination of water for possible human consumption,
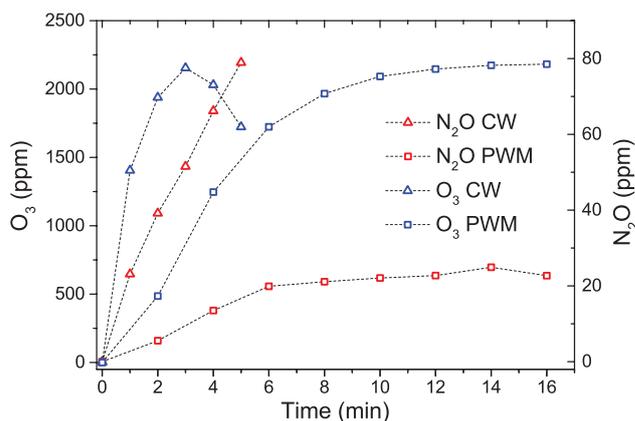
such changes to the liquid are highly undesirable. To overcome this, pulse modulation of the discharge on a millisecond time-scale was employed. Olszewski *et al* showed pulse modulation to be a viable technique to prevent the transition from an oxygen dominated to nitrogen dominated gas phase chemistry. Unlike low power operation, pulse modulation has the distinct advantage that it does not compromise the spatial uniformity of the discharge along the length of the electrode strips, thus it does not compromise the convective mass transport of species away from the discharge region. Figure 6(b) shows the gas phase composition obtained at a time-averaged input power of 2.5 W (10 W input at a duty cycle of 25%), giving a time averaged power density of $0.127 \, \text{W} \cdot \text{cm}^{-2}$, putting the discharge in the oxygen dominated mode of operation.

Figure 7 shows the temporal evolution of ozone and nitrous oxide in the gas phase under both continuous and pulse modulated operation. Notably, under high-power continuous conditions, the ozone density rapidly increases to reach a maximum of 2200 ppm within 3 min, after which it rapidly decreases; a trend which is well reported in the literature [6, 24, 25]. Under low-power, pulse modulated operation, the ozone density increases at a slower rate, reaching a plateau after 14 min of operation and showing no appreciable decrease over the 16 min test duration. In contrast, nitrous oxide density increases in a linear fashion under continuous operation, reaching a maximum of 80 ppm over the duration of the test; under pulse modulated operation, nitrous oxide gradually rises to 20 ppm within 6 min followed by a plateau for the reminder of the test. It is worth noting that, long-lived RONS including ozone and nitrogen oxides that are transported through the gas phase react at the gas–liquid interface to form a rich variety of potent antimicrobial species. The penetration of these species on to the bulk liquid is limited to the interface region, with computational studies of species transport through the aqueous medium indicating that many species are confined to the first few nanometers of the liquid [14]. Critically, the long-lived plasma generated species arriving at the gas–liquid interface are important precursors for the production of reactive species in the liquid phase species such as hydroxyl radicals and aqueous nitric oxide, both of which are known to have powerful antimicrobial properties [14].
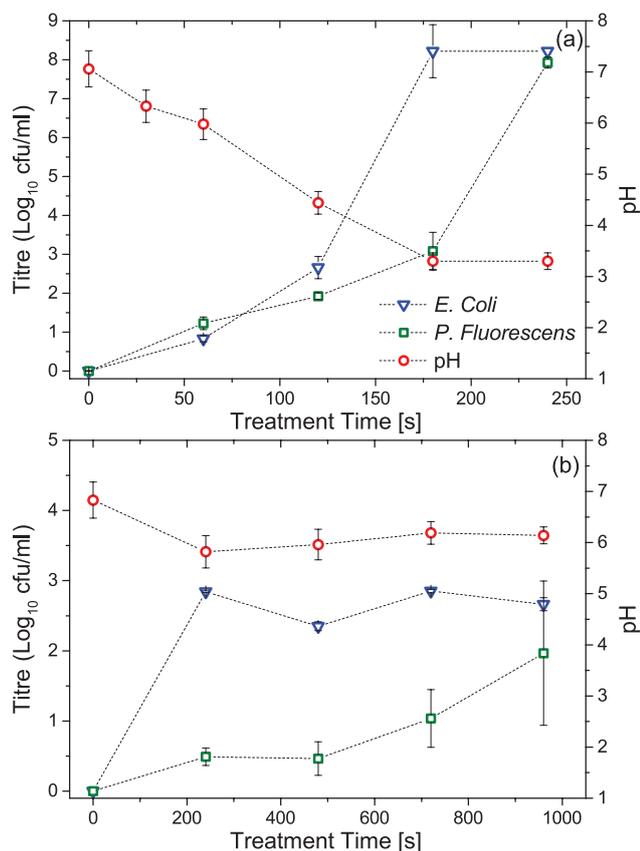
Figure 8. Microbial log reduction and pH in (a) continuous operation ($0.51 \, W \cdot cm^{-2}$) and (b) pulse modulated operation ($0.13 \, W \cdot cm^{-2}$).

4.3. Microbial decontamination

It is evident from the temporal evolution of the ozone and nitrous oxide density, shown in figure 7, that the gas phase chemistry varies significantly with the discharge mode of operation and is non-stationary in time; consequently, any microbial decontamination effect observed is likely to be attributed to the combined effect of both the reactive oxygen and nitrogen species. The decontamination efficiency of the device is highlighted in figure 8 which shows the number of viable bacterial colonies present in autoclaved potable water inoculated with *E. coli* and *Pseudomonas fluorescens* with a starting concentration of $1 \times 10^8 \, CFU \cdot ml^{-1}$ and subjected to plasma treatments of varying duration. The impact of high-power, continuous, plasma operation is shown in figure 8(a) along with the pH of the solution measured at the end of each test. For both *E. coli* and *P. fluorescens*, a 4 min exposure time was sufficient to yield the maximum 8 log reduction in the number of viable bacterial colonies. Notably, an abrupt jump in the level of inactivation is observed between 3 and 4 min for *E. coli* and 4 to 5 min for *P. fluorescens*. The change in pH of the treated solution can be used to explain this discontinuity in the inactivation curve, as it is well known that *P. fluorescens* and *E. coli* are sensitive to pHs below 4 [14, 27]. During short treatment times, where the pH remains above 4, relatively modest log reductions are observed (1.92 and 2.65 log reductions for *P. fluorescens* and *E. coli*, respectively, following 120 s

of plasma exposure). In contrast, low-power, pulse modulated operation shows a significantly lower level of inactivation, with a maximum 2.85 log reduction of *E. coli* and 1.97 log reduction of *P. fluorescens* observed. Under these plasma generation conditions, the pH shows only a minor decrease from 6.8 to ⌣6; thus any microbial inactivation cannot be attributed to acidification of the solution. Interestingly, the level of inactivation observed in the pulse modulated case is consistent with that observed during short exposures to the high-power discharge. Based on the temporal evolution of gas phase species shown in figure 7, it is clear that the gas phase composition in the pulse modulated case is similar to that observed in the first 2 min of continuous discharge case (with high ozone concentration and low nitrous oxide concentration) thus indicating that ozone is one of the major inactivation pathways under neutral and weakly acidic conditions (pH 4.5); such observations are in line with those presented by Pavlovich *et al* where aqueous-phase ozone was identified as the dominant inactivation mechanism [4]. At lower pH values, the enhanced decontamination has been linked to synergistic effects such as the increased production of hydroperoxyl and peroxynitrite radicals, both of which are readily able to penetrate cellular membranes and damage bacteria [14].

5. Concluding remarks

This contribution details the development and characterisation of a portable plasma device that is suitable for the decontamination of liquids without the need for any external power source or additional gas supply. The device is based on an efficient switched mode power supply which is powered by a battery charged from an integrated solar cell. Using PIV to visualise air flows around the device, the geometry of the plasma generating electrode unit was enhanced to produce an air flow of ⌣ $0.5 \, m \cdot s^{-1}$ perpendicular to the discharge electrode. It is proposed that this enhanced and directed flow is able to increase the mass transport of plasma species through the gas phase to a sample placed downstream. Using FTIR analysis it was observed that the gas phase composition can vary significantly depending on the plasma generation conditions; enabling the composition of the gas phase chemistry to be manipulated electrically. Using pulse-modulation of the driving waveform it was demonstrated that an abundance of reactive oxygen species (notably ozone) can be produced with minimal associated production of reactive nitrogen species.

In the context of portable water production from contaminated sources, a significant reduction in the pH of the treated solution is highly undesirable; thus low-power or pulse-modulated operation are the only viable modes of operation. Low-power operation has the disadvantage of producing a non-homogeneous discharge which only partially covers the electrode area, thus compromising the generation of air flows from the device. Desirable discharge chemistries can be achieved using pulsed modulated operation, without compromising the discharge uniformity and therefore flow characteristics.

It was demonstrated that microbial decontamination in a relatively large liquid volume (25 ml) is primarily correlated with

J. Phys. D: Appl. Phys. 49 (2016) 355203

Y Ni et al

ozone production in the pulse modulated mode of operation; similarly, short exposures to the plasma operating in a continuous mode of operation showed a similar level of antimicrobial efficacy. Under high power operation it is proposed that acidification of the liquid plays a key role in inactivation. Critically, in the pulse modulated mode of operation inactivation is limited by the mass transfer of reactive oxygen species (primarily ozone) from the plasma region to the liquid phase. In the context of liquid decontamination, simply increasing the discharge power to increase the density of reactive oxygen species is not a sustainable approach due to the increased production of undesirable reactive nitrogen species and the ultimate acidification of the solution. Possible solutions to this challenge could be to further manipulate the plasma generating waveform (for example by using shorter duration, higher-power pulses), or, by further enhancing the geometry of the electrode structure to produce flows $\gg 1 \, \mathrm{m \cdot s^{-1}}$, thus significantly increasing transport of short-lived plasma species, such as hydroxyl radicals, to the liquid surface. Overall, the prototype plasma device developed shows great promise for the 'consumable-free' decontamination of water. Following optimisation of the device to increase both the throughput and inactivation efficacy a thorough toxicological assessment of the treated water would be essential to identify any potentially harmful remnant chemical species in the liquid. Only when the portability of the treated water can be assured could such a system be deployed in the field.

Acknowledgments

References

[1] Kong M G, Kroesen G, Morfill G, Nosenko T, Shimizu T, van Dijk J and Zimmermann J L 2009 Plasma medicine: an introductory review *New J. Phys.* **11** 115012
[2] Bayliss D L, Walsh J L, Shama G, Iza F and Kong M G 2009 Reduction and degradation of amyloid aggregates by a pulsed radio-frequency cold atmospheric plasma jet *New J. Phys.* **11** 115024
[3] Cooper M, Fridman G, Staack D, Gutsol A F, Vasilets V N, Anandan S, Cho Y I, Fridman A and Tsapin A 2009 Decontamination of surfaces from extremophile organisms using nonthermal atmospheric-pressure plasmas *IEEE Trans. Plasma Sci.* **37** 866–71
[4] Pavlovich M J, Chang H-W, Sakiyama Y, Clark D S and Graves D B 2013 Ozone correlates with antibacterial effects from indirect air dielectric barrier discharge treatment of water *J. Phys. D: Appl. Phys.* **46** 145202
[5] Malik M, Ghaffar A and Malik S 2001 Water purification by electrical discharges *Plasma Sources Sci. Technol.* **10** 82–91

[6] Olszewski P, Li J F, Liu D X and Walsh J L 2014 Optimizing the electrical excitation of an atmospheric pressure plasma advanced oxidation process *J. Hazard. Mater.* **279** 60–6
[7] Locke B R, Sato M, Sunka P, Hoffmann M R and Chang J S 2006 Electrohydraulic discharge and nonthermal plasma for water treatment *Ind. Eng. Chem. Res.* **45** 882–905
[8] Prüss-Üstün A, Bos R, Gore F and Bartram J 2008 *Safer Water, Better Health: Costs, Benefits and Sustainability of Interventions to Protect and Promote Health* (Geneva: World Health Organization)
[9] World Health Organization and UNICEF 2012 Progress on Drinking Water and Sanitation: 2012 Update
[10] Walsh J L and Kong M G 2008 Atmospheric dielectric-barrier discharges scalable from 1 mm to 1 m *IEEE Trans. Plasma Sci.* **36** 1314–5
[11] Parkey J, Cross J, Hayes R, Parham C, Staack D and Sharma A C 2015 A battery powered, portable, and self-contained nonthermal helium plasma jet device for point-of-injury burn wound treatment *Plasma Process. Polym.* **12** 1244–55
[12] Walsh J L and Kong M G 2011 Portable nanosecond pulsed air plasma jet *Appl. Phys. Lett.* **99** 081501
[13] Pei X, Liu J, Xian Y and Lu X 2014 A battery-operated atmospheric-pressure plasma wand for biomedical applications *J. Phys. D: Appl. Phys.* **47** 145204
[14] Liu Z C, Liu D X, Chen C, Li D, Yang A J, Rong M Z, Chen H L and Kong M G 2015 Physicochemical processes in the indirect interaction between surface plasma and deionized water *J. Phys. D: Appl. Phys.* **48** 495201
[15] Westerweel J 1997 Fundamentals of digital particle image velocimetry *Meas. Sci. Technol.* **8** 1379–92
[16] Tropea C, Yarin A and Foss J 2007 *Springer Handbook of Experimental Fluid Mechanics* (New York: Springer)
[17] American Public Health Association Assn 1999 *Standard Methods for the Examination of Water and Wastewater* ed A D Eaton *et al* (Washington, DC: American Public Health Association)
[18] Sharpe S, Sams R L and Johnson T J 2002 The PNNL quantitative IR database for infrared remote sensing and hyperspectral imaging *Applied Imagery Pattern Recognition Workshop, Proc.* (Washington, DC: IEEE Computer Society) pp 45–8
[19] Sakiyama Y, Graves D B, Chang H-W, Shimizu T and Morfill G E 2012 Plasma chemistry model of surface microdischarge in humid air and dynamics of reactive neutral species *J. Phys. D: Appl. Phys.* **45** 425201
[20] Wang J-J, Choi K-S, Feng L-H, Jukes T N and Whalley R D 2013 Recent developments in DBD plasma flow control *Prog. Aerosp. Sci.* **62** 52–78
[21] Boeuf J P, Lagmich Y, Unfer T, Callegari T and Pitchford L C 2007 Electrohydrodynamic force in dielectric barrier discharge plasma actuators *J. Phys. D: Appl. Phys.* **40** 652–62
[22] Whalley R D and Choi K-S 2012 The starting vortex in quiescent air induced by dielectric-barrier-discharge plasma *J. Fluid Mech.* **703** 192–203
[23] Whalley R and Choi K-S 2010 Starting, traveling, and colliding vortices: dielectric-barrier-discharge plasma in quiescent air *Phys. Fluids* **22** 091105
[24] Shimizu T, Sakiyama Y, Graves D B, Zimmermann J L and Morfill G E 2012 The dynamics of ozone generation and mode transition in air surface micro-discharge plasma at atmospheric pressure *New J. Phys.* **14** 103028
[25] Pavlovich M J, Clark D S and Graves D B 2014 Quantification of air plasma chemistry for surface disinfection *Plasma Sources Sci. Technol.* **23** 065036
[26] Eliasson B and Kogelschatz U 1991 Modeling and applications of silent discharge plasmas *IEEE Trans. Plasma Sci.* **19** 309–23
[27] Foster J W 2004 *Escherichia coli* acid resistance: tales of an amateur acidophile *Nat. Rev. Microbiol.* **2** 898–907